Solid State Sciences 12 (2010) 345–349

Contents lists available at ScienceDirect

Solid State Sciences

journal homepage: www.elsevier.com/locate/ssscie

Synthesis and characterization of nanoporous $NaYF_4:Yb^{3+}$, $Tm^{3+}@SiO_2$ nanocomposites

Lina Liu [a,b], Bin Li [a,*], Ruifei Qin [a,b], Haifeng Zhao [a], Xinguang Ren [a], Zhongmin Su [c,**]

[a] Key Laboratory of Excited State Physics, Changchun Institute of Optics, Fine Mechanics and Physics, Chinese Academy of Sciences, 16 Eastern South-Lake Road, Changchun 130033, PR China
[b] Graduate School of the Chinese Academy of Sciences, Chinese Academy of Sciences, Beijing 100039, PR China
[c] Polyoxometalate Science Key Laboratory of Ministry of Education, Faculty of Chemistry, Northeast Normal University, Changchun 130024, PR China

ARTICLE INFO

Article history:
Received 18 September 2009
Received in revised form
16 November 2009
Accepted 20 November 2009
Available online 26 November 2009

Keywords:
Nanoporous
Nanocomposites
$NaYF_4:Yb^{3+}Tm^{3+}$
Upconversion

ABSTRACT

Novel upconversion nanocomposites with nanoporous structure were presented in this paper. Silica-coated cubic $NaYF_4:Yb^{3+}$, Tm^{3+} nanoparticles were first prepared. After annealing, monodisperse cubic/hexagonal mixed phases $NaYF_4:Yb^{3+}$, $Tm^{3+}@SiO_2$ nanoparticles were obtained, and the $NaYF_4:Yb^{3+}$, Tm^{3+} cores became nanoporous. To the best of our knowledge, the nanoporous structure in $NaYF_4:Yb^{3+}$, $Tm^{3+}@SiO_2$ nanocomposites was observed for the first time. They demonstrate increased upconversion emission compared with unannealed dense $NaYF_4:Yb^{3+}$, Tm^{3+} nanoparticles due to the appearance of the hexagonal $NaYF_4:Yb^{3+}$, Tm^{3+}. The silica shell not only makes the nanocomposites possess bio-affinity but also protects the $NaYF_4:Yb^{3+}$, Tm^{3+} cores from aggregating and growing up. Thus the upconversion, nanoporous and bio-affinity properties were combined into one single nanoparticle. The nanocomposites have been characterized by X-ray diffraction (XRD), field-emission scanning electron microscopy (FE-SEM), transmission electron microscopy (TEM), small angle X-ray diffraction (SAXRD) and emission spectroscopy. These multifunctional nanocomposites are expected to find applications in biological fields, such as biolabels, drug storage and delivery.

1. Introduction

Nanocomposite materials [1–6] provide the possibility for enhanced functionality and multifunctional properties in contrast with their more-limited single-component counterparts. One example of nanocomposite materials is the core/shell structure. The lanthanide ions (Ln^{3+}, Ln = Er, Tm, and Yb) doped upconversion nanocrystals have attracted significant interest due to their many potential biological applications [7–9]. Compared with conventional downconversion fluorescent labels [10–12] which require an ultra-violet or blue excitation wavelength, upconversion nanocrystals have many conceivable advantages as fluorescence labeling materials including an improved signal-to-noise ratio due to the absence of autofluorescence and reduction of light scattering [13,14], carrying out easily in vivo imaging upon the NIR (near infrared) irradiation with noninvasive and deep penetration to the tissue or cell [15], low photobleaching [16] and feasibility of multiple labeling with different emissions under the same excitation. A compact, power-rich, and inexpensive 980 nm near infrared laser may be used as the excitation source. Up to now, among the various host materials for upconversion, hexagonal $NaYF_4$ (β-$NaYF_4$) has been reported as the most efficient host matrix for green and blue upconversion when activated by Yb^{3+} and Er^{3+}/Tm^{3+} ions due to the very low phonon energy of its lattice [17,18]. Many methods have been used to prepare hexagonal $NaYF_4$ [19–23], but the products prepared by those methods were usually big or hydrophobic, having adverse effect on biologic applications. Cubic $NaYF_4$ can turn into hexagonal $NaYF_4$ through annealing [24], but in general, annealing makes nanoparticles aggregate and grow up. In this paper, silica-coated cubic $NaYF_4:Yb^{3+}$, Tm^{3+} nanoparticles were first prepared and then annealed at 500 °C for 3 h. Nearly monodisperse $NaYF_4:Yb^{3+}$, $Tm^{3+}@SiO_2$ nanoparticles were obtained. No aggregation and growing up of $NaYF_4:Yb^{3+}$, Tm^{3+} cores occurred. A part of cubic $NaYF_4:Yb^{3+}$, Tm^{3+} turned into hexagonal $NaYF_4:Yb^{3+}$, Tm^{3+}, increasing the upconversion emission of $NaYF_4:Yb^{3+}$, Tm^{3+}. Interestingly, the $NaYF_4:Yb^{3+}$, Tm^{3+} cores became nanoporous after annealing. As our knowledge, nanoporous structure in $NaYF_4:Yb^{3+}$, Tm^{3+} cores was found for the first time, making them possess some new potential biological applications, such as drug storage and delivery [25,26]. The surface of silica is easily conjugated with amines, thiols and carboxyl groups, which in turn would facilitate the linking of biomolecules

* Corresponding author. Fax: +86 431 6176935.
** Corresponding author.
E-mail address: lib020@ciomp.ac.cn (B. Li).

1293-2558/$ – see front matter © 2009 Elsevier Masson SAS. All rights reserved.
doi:10.1016/j.solidstatesciences.2009.11.011

such as biotin and avidin. On the basis of the above analysis, novel multifunctional nanocomposite materials possessing upconversion, nanoporous, and bio-affinity properties were reported in this paper. The silica shells not only make the nanocomposites possess bio-affinity but also protect the $NaYF_4$:Yb^{3+}, Tm^{3+} cores from aggregating and growing up. These multifunctional nanocomposites are expected to find applications in biochemical and biomedical fields.

2. Experimental section

2.1. Synthesis

All chemicals were of analytical grade and were used as received. Deionized water was used throughout. The synthesis procedure of nanocomposite materials is shown in Fig. 1. $NaYF_4$:Yb^{3+}, Tm^{3+} nanoparticles were first prepared by a solvothermal method. Then tetraethoxysilane (TEOS) hydrolyzed on the surface of $NaYF_4$:Yb^{3+}, Tm^{3+} to form the silica shell. At last, porous and upconversion emission enhanced $NaYF_4$:Yb^{3+}, Tm^{3+}@SiO_2 nanocomposites were obtained through annealing.

$NaYF_4$:Yb^{3+}, Tm^{3+} nanoparticles were synthesized using a previously described procedure with a slight modification [27]. An aqueous solution of $Y(NO_3)_3$, $Yb(NO_3)_3$ and $Tm(NO_3)_3$ (lanthanide ion molar ratio, Y/Yb/Tm = 74.7:25:0.3) was mixed with an aqueous solution of ethylenediamine tetraacetic acid disodium salt (EDTA) under vigorous stirring, resulting in a white complex. An aqueous solution of NaF was added into the complex and stirred for 1 h. The lanthanide/EDTA/NaF molar ratio is 1/1/12 and the lanthanide ions concentration in the resulting precursor solution is 0.02 mol/L. The resulted precursor solution was transferred to a 50 mL autoclave. The autoclave was then placed in a digital type temperature controlled oven and heated at 180 °C for 2 h, and then allowed to cool down to room temperature naturally. Subsequently, the precipitate of $NaYF_4$:Yb^{3+}, Tm^{3+} nanoparticles in the autoclave could be separated from the reaction media by centrifugation and then washed with deionized water and ethanol for several times. After being dried in vacuum at 80 °C for 3 h, $NaYF_4$:Yb^{3+}, Tm^{3+} nanoparticles (denoted as sample NYF-1) were obtained. For comparison purpose, sample NYF-2 was synthesized through sintering sample NYF-1 at 500 °C for 3 h.

$NaYF_4$:Yb^{3+}, Tm^{3+}@SiO_2 core/shell nanoparticles were prepared by a modified stöber method. 30 mg $NaYF_4$:Yb^{3+}, Tm^{3+} nanoparticles were dispersed in 80 mL 2-propanol by sonication for 30 min. Then 8.94 mL 28% ammonia, 7.5 mL deionized water, and 0.1 mL TEOS were added into the mixture. The mixture was then placed into an ultrasonic bath and kept for 2 h. The product was collected, washed and dried as sample NYF-1. The obtained product was labeled as sample NYF-SO-1. Sample NYF-SO-2 was obtained through sintering sample NYF-SO-1 at 500 °C for 3 h.

2.2. Measurements

The data of X-ray diffraction (XRD) patterns were obtained on a Rigaku D/Max-Ra X-ray diffractometer using a Cu target radiation source ($\lambda = 1.5418$ Å). The field-emission scanning electron microscopy (FE-SEM) and transmission electron microscopy (TEM) images were measured on a Hitachi S-4800 microscope and a JEM-2010 transmission election microscope, respectively. The small angle X-ray diffraction (SAXRD) pattern was obtained on a Rigaku-Dmax 2500 diffractometer using Cu KR radiation (40 kV, 200 mA) at a step width of 0.05°. The upconversion fluorescence spectra were obtained on a Hitachi F-4500 fluorescence spectrophotometer under the excitation of a 980 nm laser diode.

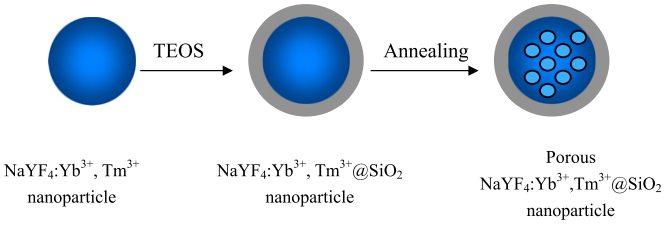

Fig. 1. Schematic diagram of synthetic procedure.

3. Results and discussion

3.1. XRD patterns

XRD patterns of various samples are presented in Fig. 2. Before annealing, all diffraction peaks for samples NYF-1 and NYF-SO-1 could be readily indexed to the cubic phase of $NaYF_4$ according to the Joint Committee on Powder Diffraction Standards (JCPDS) file no. 77-2042. The same XRD patterns of samples NYF-1 and NYF-SO-1 indicated that the silica shell was amorphous. As shown in Fig. 2, after annealing, some diffraction peaks of hexagonal $NaYF_4$ appeared in the XRD pattern of sample NYF-SO-2. Hexagonal $NaYF_4$ formed in the annealing process and it is the main reason for enhanced upconversion emission of sample NYF-SO-2.

3.2. SEM, TEM images and SAXRD pattern

The $NaYF_4$:Yb^{3+}, Tm^{3+} nanoparticles with an average diameter of 110 nm obtained by hydrothermal method are uniform and monodisperse (sample NYF-1, Fig. 3a), making the next coating procedure possible. The SEM image of sample NYF-SO-1 is shown in Fig. 3b. The core/shell structure is obviously observed and the nanoparticles are nearly monodisperse. The SEM images of samples NYF-2 and NYF-SO-2 are shown in Fig. 3c and d, respectively. It is found that the $NaYF_4$:Yb^{3+}, Tm^{3+} nanoparticles in sample NYF-2 aggregate seriously, distort and are hardly identified. Contrarily, compared with sample NYF-2, the nanoparticles in sample NYF-SO-2 hardly aggregate (Fig. 3d). Samples NYF-2 and NYF-SO-2 were obtained through annealing samples NYF-1 and NYF-SO-1, respectively. Sample NYF-SO-1 was coated with SiO_2 shell, but sample NYF-1 was bare $NaYF_4$:Yb^{3+}, Tm^{3+}. Thus we deduce that the SiO_2 shell protects $NaYF_4$:Yb^{3+}, Tm^{3+} cores from aggregating and growing up. The monodisperse property is crucial for biological applications. The silica shell can also make the nanocomposites

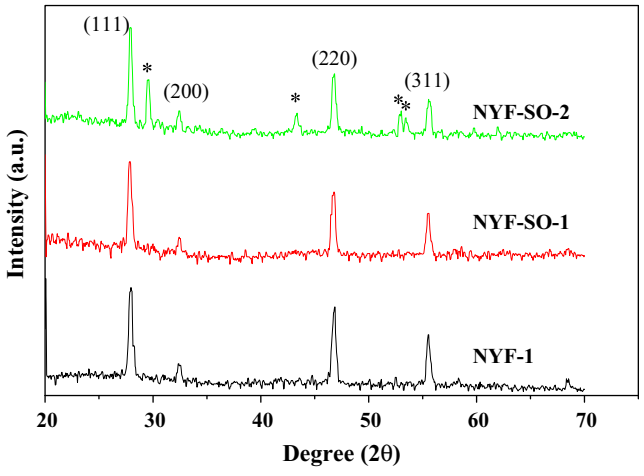

Fig. 2. XRD patterns of samples NYF-1, NYF-SO-1 and NYF-SO-2. The peaks marked with asterisks (*) are the diffraction peaks of hexagonal $NaYF_4$:Yb^{3+}, Tm^{3+}.

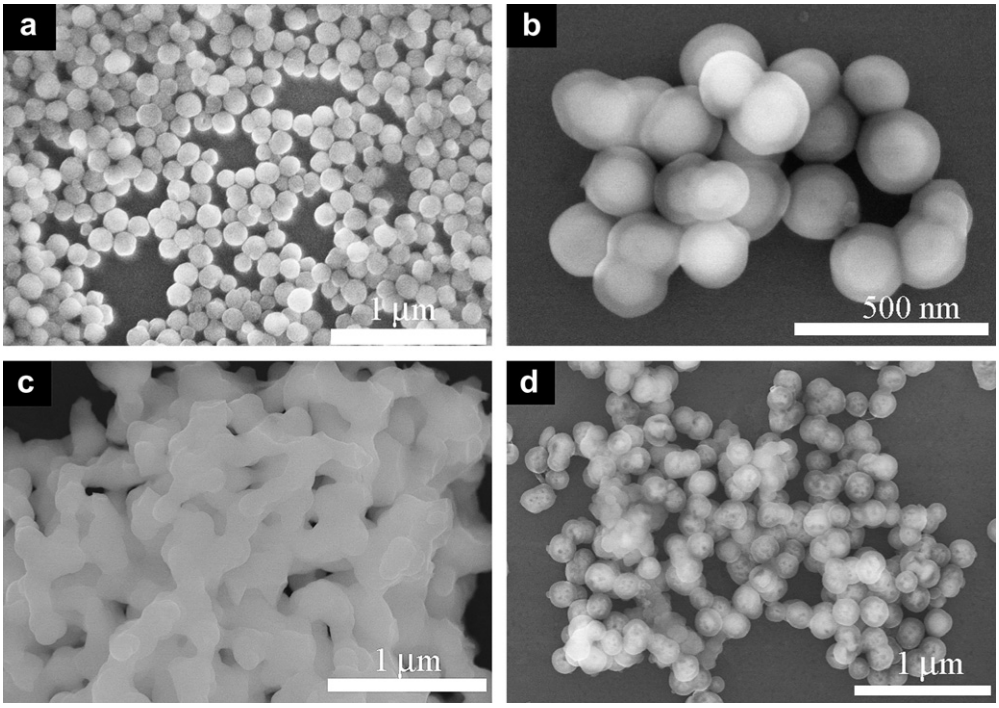

Fig. 3. SEM images of (a) sample NYF-1, (b) sample NYF-SO-1, (c) sample NYF-2, and (d) sample NYF-SO-2.

possess bio-affinity property [28–30]. From Fig. 3d we can see that the surfaces of the $NaYF_4$:Yb^{3+}, Tm^{3+} cores after annealing were not as smooth as those of the $NaYF_4$:Yb^{3+}, Tm^{3+} cores before annealing. In order to characterize the core/shell structure and the morphologies of the $NaYF_4$:Yb^{3+}, Tm^{3+} cores after annealing, TEM images of sample NYF-SO-2 are shown in Fig. 4a and b. It can be clearly observed that the nanocomposites have a core/shell structure and the silica shell is clearly visible. The thickness of the silica shells is uniform (~30 nm), and the shell surface appears to be quite smooth. Moreover, the shell thickness can be adjusted by

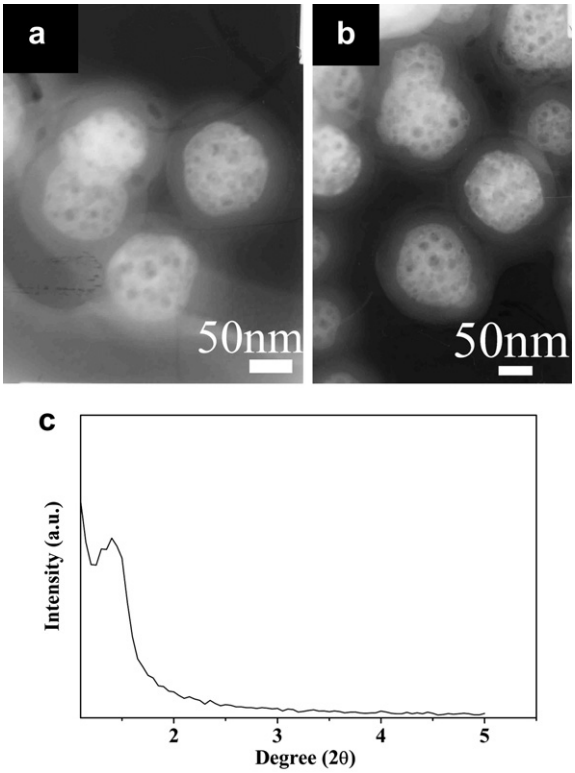

Fig. 4. (a), (b) TEM images and (c) SAXRD pattern of sample NYF-SO-2.

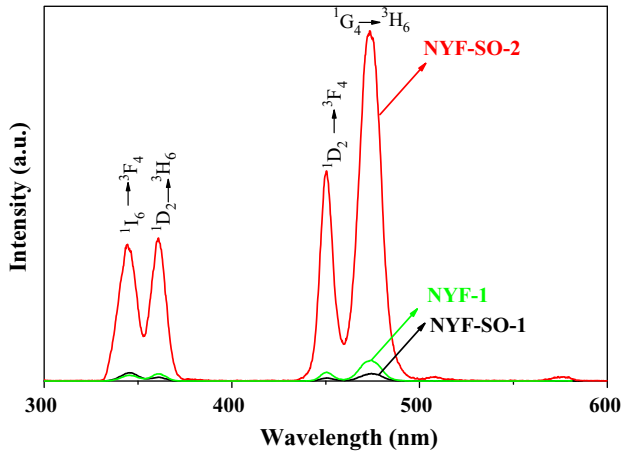

Fig. 5. The upconversion spectra of samples NYF-1, NYF-SO-1 and NYF-SO-2 under 980 nm laser diode excitation.

changing the concentration of TEOS and the reaction time [31]. Interestingly, as shown in Fig. 4, annealing makes the $NaYF_4$:Yb^{3+}, Tm^{3+} cores nanoporous. Fig. 4c shows the SAXRD pattern of sample NYF-SO-2. A broad Bragg reflection peak at about 1.4° was found, indicating the ordering degree of the nanopores. The nanoporous property of the nanocomposites makes them possess some new potential biological applications, such as drug storage and delivery. $NaYF_4$:Yb^{3+}, Tm^{3+} cores will deform and grow up in the annealing process if SiO_2 shells do not exist. In the core/shell nanocomposites, the SiO_2 shells restrict growing up of the cores, and the cores only can deform inside the shells. The deformation of $NaYF_4$:Yb^{3+}, Tm^{3+} units in one core is not uniform and not towards just one direction. Therefore, the nanopores formed. The SiO_2 shell and anneal play important roles in the formation of nanoporous core.

3.3. Upconversion emission spectra and mechanism

Fig. 5 shows the room temperature upconversion emission spectra of samples NYF-1, NYF-SO-1 and NYF-SO-2 in the 300–600 nm wavelength range, recorded under 980 nm excitation. There are four emission peaks at 346, 361, 450, 474 nm, which are assigned to the $^1I_6 \rightarrow {}^3F_4$, $^1D_2 \rightarrow {}^3H_6$, $^1D_2 \rightarrow {}^3F_4$, $^1G_4 \rightarrow {}^3H_6$

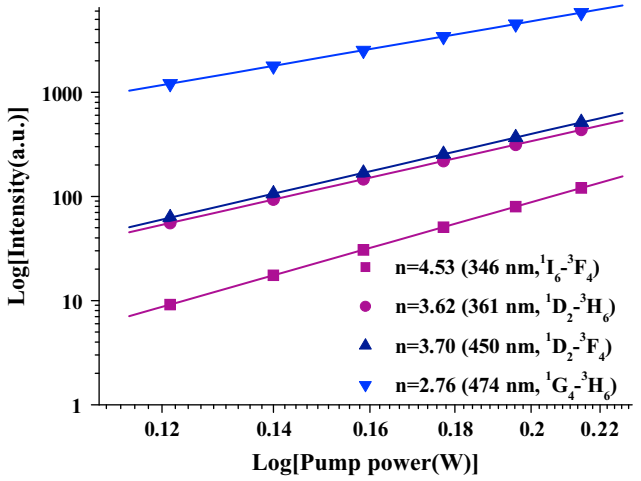

Fig. 6. Plots of logarithm intensity of the upconversion emissions versus logarithm pump power of diode laser at 346 nm (■), 361 nm (●), 450 nm (▲) and 474 nm (▼) for sample NYF-SO-2.

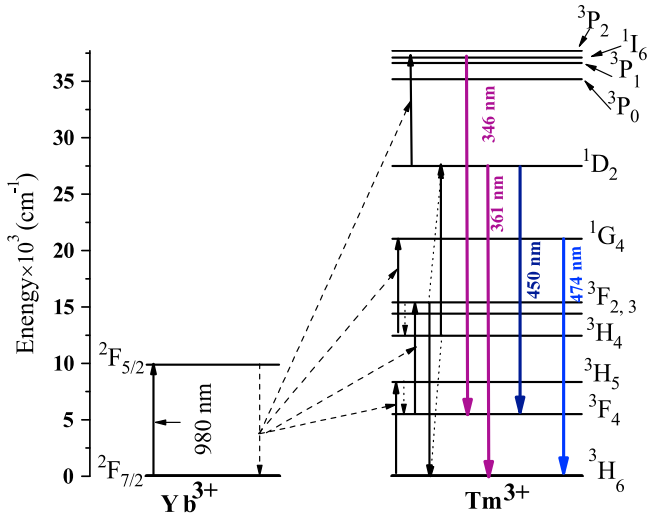

Fig. 7. The energy level diagrams of the Tm^{3+} and Yb^{3+} dopant ions and upconversion mechanism following 980 nm laser diode excitation. The full, dashed and dotted arrows represent emission, energy transfer and multiphonon relaxation processes, respectively.

transitions of Tm^{3+} [32]. Only the peaks at 450 and 474 nm are in the visible range, which makes the samples appear bright blue when pumped by the 980 nm laser. The upconversion emission of sample NYF-SO-2 is much stronger than those of samples NYF-1 and NYF-SO-1 due to the existence of hexagonal $NaYF_4$:Yb^{3+}, Tm^{3+} in sample NYF-SO-2. The intensity of the 346 nm emission peak is weaker than that of the 361 nm emission peak in sample NYF-1. However, contrary result is observed for sample NYF-SO-1. Silica coating can change the surface properties of $NaYF_4$:Yb^{3+}, Tm^{3+} nanoparticles. Furthermore, the silica shell may reflect some peaks of the upconversion emission and aggregate the 980 nm laser. All the above-mentioned cases can alter the intensity ratios of the upconversion emission peaks [33,34]. Dependence of the upconversion luminescence intensity on pump power was performed to obtain a better understanding of the upconversion process. For unsaturated upconversion luminescence, the emission intensity, I_{em}, is proportional to $(I_{ex})^n$, i.e., $I_{em} \propto (I_{ex})^n$, where I_{ex} is the excitation intensity and the integer n is the number of photons required to populate the emitting state, which can be determined from the slope of a Log–Log plot of the upconversion intensity versus pump power [35]. Fig. 6 shows the double logarithmic plots of the emission intensity as a function of excitation power for the aforementioned four emission transitions in sample NYF-SO-2. The slopes of the linear fittings are 4.53 for $^1I_6 \rightarrow {}^3F_4$, 3.62 for $^1D_2 \rightarrow {}^3H_6$, 3.70 for $^1D_2 \rightarrow {}^3F_4$ and 2.76 for $^1G_4 \rightarrow {}^3H_6$, indicating that five, four and three pumping photons are required to populate the $^1I_6$, $^1D_2$ and $^1G_4$ emitting levels, respectively. The possible upconversion mechanism of the $NaYF_4$:Yb^{3+}, Tm^{3+} nanoparticles is presented in Fig. 7 [36,37]. Under the 980 nm excitation, electron of Yb^{3+} was excited from $^2F_{7/2}$ to $^2F_{5/2}$ level. The electrons on ground states $^3H_6$ are excited to $^3H_5$ through the first-step energy transfer of $Yb^{3+} \rightarrow Tm^{3+}$ and then the electrons on $^3H_5$ relax to $^3F_4$. The electrons on $^3F_4$ are excited to $^3F_2$ ($^3F_3$) through the second-step energy transfer and the electrons on $^3F_2$ ($^3F_3$) relax to $^3H_4$. The electrons on $^3H_4$ are excited to $^1G_4$ through the third-step energy transfer. There are several opinions about the population of $^1D_2$ level. Some researchers consider that the electrons on $^1G_4$ can also be excited to $^1D_2$ through the fourth-step energy transfer [38–40], but they do not give further experimental or theoretical evidences. The mismatch of energy between the $^2F_{7/2} \leftarrow {}^2F_{5/2}$ Yb^{3+} and $^1G_4 \rightarrow {}^1D_2$ Tm^{3+} transitions is about 3500 cm^{-1}, so we consider

that the fourth-step energy transfer occurs with little probability. Consequently, the cross-relaxation processes between Tm^{3+} ions play important roles in populating $^1D_2$ level. Cross-relaxation processes, such as $^3F_3 + {}^3F_3 \rightarrow {}^3H_6 + {}^1D_2$ [41,42], $^3F_2 + {}^3H_4 \rightarrow {}^3H_6 + {}^1D_2$ [43–45] as well as $^1G_4 + {}^3H_4 \rightarrow {}^3F_4 + {}^1D_2$ [37,43,45] can all populate $^1D_2$ level of Tm^{3+}. Some research groups have confirmed the rationality of aforementioned cross-relaxation processes from experimental and theoretical results [42,44–48]. Chen and his co-authors [46] consider that the population of $^1D_2$ is a five-photon process under the condition that it is populated by $^1G_4 + {}^3H_4 \rightarrow {}^3F_4 + {}^1D_2$ process. Our results indicate that the population of $^1D_2$ level is a four-photon process in sample NYF-SO-2. Therefore, we believe that the cross-relaxation processes of $^3F_2 + {}^3H_4 \rightarrow {}^3H_6 + {}^1D_2$ as well as $^3F_3 + {}^3F_3 \rightarrow {}^3H_6 + {}^1D_2$ play important roles in populating $^1D_2$ level in our samples. Only one kind of cross-relaxation process is drawn in Fig. 7. After populating the $^1D_2$ level, the electrons on $^1D_2$ level are excited to $^1I_6$ level through another energy transfer process from Yb^{3+} to Tm^{3+}. Then various emissions can occur.

4. Conclusions

In summary, multifunctional cubic/hexagonal mixed phases $NaYF_4$:Yb^{3+}, Tm^{3+}@SiO_2 nanocomposites possessing upconversion, nanoporous, and bio-affinity properties have been developed by a simple and straightforward synthetic method. The silica shell played significant roles in terms of protecting $NaYF_4$:Yb^{3+}, Tm^{3+} nanoparticles from aggregating and endowing the final materials with biocompatible properties. The annealing process not only produced hexagonal $NaYF_4$:Yb^{3+}, Tm^{3+} but also made the cores nanoporous. Various techniques have been utilized to characterize the multifunctional materials. The pores of the nanocomposites were clearly observed via TEM images and their upconversion emission was improved through annealing. They are expected to find applications in biomedical fields.

Acknowledgements

The authors gratefully thank the financial supports of One Hundred Talents Project from Chinese Academy of Sciences and the National Natural Science Foundations of China (Grant No. 50872130).

References

[1] F. Caruso, Adv. Mater. 13 (2001) 11.
[2] H. Kim, M. Achermann, L.P. Balet, J.A. Hollingsworth, V.I. Klimov, J. Am. Chem. Soc. 127 (2005) 544.
[3] Y.S. Lin, S.H. Wu, Y. Hung, Y.H. Chou, C. Chang, M.L. Lin, C.P. Tsai, C.Y. Mou, Chem. Mater. 18 (2006) 5170.
[4] N. Insin, J.B. Tracy, H. Lee, J.P. Zimmer, R.M. Westervelt, M.G. Bawendi, ACS Nano 2 (2008) 197.
[5] J. Wu, Z.Q. Ye, G.L. Wang, J.L. Yuan, Talanta 72 (2007) 1693.
[6] D. Nagao, M. Yokoyama, N. Yamauchi, H. Matsumoto, Y. Kobayashi, M. Konno, Langmuir 24 (2008) 9804.
[7] G.S. Yi, G.M. Chow, Adv. Funct. Mater. 16 (2006) 2324.
[8] W.J. Kim, M. Nyk, P.N. Prasad, Nanotechnology 20 (2009) 185301.
[9] J.W. Zhao, Y.J. Sun, X.G. Kong, L.J. Tian, Y. Wang, L.P. Tu, J.L. Zhao, H. Zhang, J. Phys. Chem. B 112 (2008) 15666.
[10] J. Feng, G.M. Shan, A. Maquieira, M.E. Koivunen, B. Guo, B.D. Hammock, I.M. Kennedy, Anal. Chem. 75 (2003) 5282.
[11] J.L. Seifert, R.E. Connor, S.A. Kushon, M. Wang, B.A. Armitage, J. Am. Chem. Soc. 121 (1999) 2987.
[12] W.J.M. Mulder, R. Koole, R.J. Brandwijk, G. Storm, P.T.K. Chin, G.J. Strijkers, C.D.M. Donegá, K. Nicolay, A.K. Griffioen, Nano Lett. 6 (2006) 1.
[13] H.J.M.A. Zijlmans, J. Bonnet, J. Burton, K. Kardos, T. Vail, R.S. Niedbala, H.J. Tanke, Anal. Biochem. 267 (1999) 30.
[14] J.A. Feijo, N. Moreno, Protoplasma 223 (2004) 1.
[15] D.K. Chatterjee, A.J. Rufaihah, Y. Zhang, Biomaterials 29 (2008) 937.
[16] W.C.W. Chan, S.M. Nie, Science 281 (1998) 2016.
[17] K.W. Krämer, D. Biner, G. Frei, H.U. Güdel, M.P. Hehlen, S.R. Lüthi, Chem. Mater. 16 (2004) 1244.
[18] A. Aebischer, M. Hostettler, J. Hauser, K. Krämer, T. Weber, H.U. Güdel, H.B. Bürgi, Angew. Chem. Int. Ed. 45 (2006) 2802.
[19] L.Y. Wang, Y.D. Li, Nano Lett. 6 (2006) 1645.
[20] H.X. Mai, Y.W. Zhang, L.D. Sun, C.H. Yan, J. Phys. Chem. C 111 (2007) 13730.
[21] C.X. Li, Z.W. Quan, J. Yang, P.P. Yang, J. Lin, Inorg. Chem. 46 (2007) 6329.
[22] H.X. Mai, Y.W. Zhang, R. Si, Z.G. Yan, L.D. Sun, L.P. You, C.H. Yan, J. Am. Chem. Soc. 218 (2006) 6426.
[23] J.L. Zhuang, L.F. Liang, H.H.Y. Sung, X.F. Yang, M.M. Wu, L.D. Williams, S.H. Feng, Q. Su, Inorg. Chem. 46 (2007) 5404.
[24] Y. Wei, F.Q. Lu, X.R. Zhang, D.P. Chen, J. Alloys Compd. 427 (2007) 333.
[25] C.H. Su, H.S. Sheu, C.Y. Lin, C.C. Huang, Y.W. Lo, Y.C. Pu, J.C. Weng, D.B. Shieh, J.H. Chen, C.S. Yeh, J. Am. Chem. Soc. 129 (2007) 2139.
[26] P.C. Wu, W.S. Wang, Y.T. Huang, H.S. Sheu, Y.W. Lo, D.B. Tsai, C.S. Yeh, Chem. Eur. J. 13 (2007) 3878.
[27] Y.J. Sun, Y. Chen, L.J. Tian, Y. Yu, X.G. Kong, J.W. Zhao, H. Zhang, Nanotechnology 18 (2007) 275609.
[28] M.J. Li, Z.F. Chen, V.W.W. Yam, Y.B. Zu, ACS Nano 2 (2008) 905.
[29] Z.Y. Liu, G.S. Yi, H.T. Zhang, J. Ding, Y.W. Zhang, J.M. Xue, Chem. Commun. 26 (2008) 694.
[30] H.C. Lu, G.S. Yi, S.Y. Zhao, D.P. Chen, L.H. Guo, J. Cheng, J. Mater. Chem. 14 (2004) 1336.
[31] M. Ohmori, E. Matijević, J. Colloid Interf. Sci. 150 (1992) 594.
[32] G.J.H. De, W.P. Qin, W.H. Wang, B. Gui, Opt. Commun. 282 (2009) 2950.
[33] Z.Q. Li, Y. Zhang, Angew. Chem. Int. Ed. 45 (2006) 7732.
[34] J.N. Shan, Y.G. Ju, Appl. Phys. Lett. 91 (2007) 123103.
[35] M. Pollnau, D.R. Gamellin, S.R. Lüthi, H.U. Güdel, Phys. Rev. B 61 (2000) 3337.
[36] B. Dong, H.W. Song, H.Q. Yu, H. Zhang, R.F. Qin, X. Bai, G.H. Pan, S.Z. Lu, F. Wang, L.B. Fan, Q.L. Dai, J. Phys. Chem. C 112 (2008) 1435.
[37] G.F. Wang, W.P. Qin, J.S. Zhang, L.L. Wang, G.D. Wei, P.F. Zhu, R.J. Kim, J. Alloys Compd. 475 (2009) 452.
[38] L.Y. Wang, Y.D. Li, Chem. Mater. 19 (2007) 727.
[39] F. Vetrone, V. Mahalingam, J.A. Capobianco, Chem. Mater. 21 (2009) 1847.
[40] J.F. Suyver, A. Aebischer, D. Biner, P. Gerner, J. Grimm, S. Heer, K.W. Krämer, C. Reinhard, H.U. Güdel, Opt. Mater. 27 (2005) 1111.
[41] C.Y. Cao, W.P. Qin, J.S. Zhang, Y. Wang, P.F. Zhu, G.F. Wang, G.D. Wei, L.L. Wang, L.Z. Jin, J. Fluorine Chem. 129 (2008) 204.
[42] R.J. Thrash, L.F. Johnson, J. Opt. Soc. Am. B 11 (1994) 881.
[43] D.Q. Chen, Y.S. Wang, Y.L. Yu, P. Huang, Appl. Phys. Lett. 91 (2007) 051920.
[44] G.F. Wang, W.P. Qin, J.S. Zhang, J.S. Zhang, Y. Wang, C.Y. Cao, L.L. Wang, G.D. Wei, P.F. Zhu, R.J. Zhu, J. Phys. Chem. C 112 (2008) 12161.
[45] G.F. Wang, W.P. Qin, L.L. Wang, G.D. Wei, P.F. Zhu, R.J. Kim, Opt. Express 16 (2008) 11907.
[46] X.B. Chen, Z.F. Song, J. Opt. Soc. Am. B 24 (2007) 965.
[47] M.A. Noginov, M. Curley, P. Venkateswarlu, A. Williams, J. Opt. Soc. Am. B 14 (1997) 2126.
[48] G.Y. Chen, G. Somesfalean, Z.G. Zhang, Q. Sun, F.P. Wang, Opt. Lett. 32 (2007) 87.